RANGE MULTIPATH REDUCTION IN PLANE-POLAR NEAR-FIELD ANTENNA MEASUREMENTS

Stuart Gregson, Allen Newell, Greg Hindman, Pat Pelland
Nearfield Systems Inc.
19730 Magellan Drive,
Torrance, CA 90502-1104

ABSTRACT

This paper details a recent advance that, for the first time, enables the Mathematical Absorber Reflection Suppression (MARS) technique to be successfully deployed to correct measurements taken using plane-polar near-field antenna test systems with reduced AUT-to-probe separation. This paper provides an overview of the measurement, transformation, and post-processing. Preliminary results of range measurements are presented and discussed that illustrate the success of the new plane-polar MARS technique by utilising redundancy within the near-field measured data that enables comparisons to be obtained and verified by using two existing, alternative, scattering suppression methodologies.

Keywords: Reflection Suppression, Plane-Polar, Near-field, Antenna Measurements, Cylindrical Wave Expansion.

1. Introduction

During the past three decades, planar near-field antenna measurements have developed to become arguably the most frequently harnessed technique for characterising electrically large, medium to high gain, antennas [1]. The comparative popularity of this technique perhaps stems from its particular set of attributes which include: the ability for the AUT to remain at rest during the measurement, the comparatively straightforward theoretical basis, and the highly efficient and numerically stable transformation algorithm. Generally, amplitude and phase data are recorded at regular intervals across a rectilinear raster grid. However, although the plane rectilinear geometry is by far the most commonly encountered implementation, plane-polar [2] and plane-bipolar [3] geometries can also be constructed using mechanically convenient commercially available positioning equipment. The plane-polar near-field measurement system is formed from the intersection of a linear translation stage and a rotation stage. The combination of the rotation and linear axes enable the probe to trace out a radial vector in two-dimensions thereby enabling the collection of samples across the surface of a plane on a set of concentric rings. Here, samples are taken at regular intervals across a polar grid with, typically, the probe moving in a fixed radial direction and the AUT rotating axially. In addition to yielding a simplification to the positioning and RF subsystems, a crucial feature of the technique is the ability of the scan plane diameter to be as much as twice as large as the length of the linear probe scanning axis. Thus, this enables measurements to be taken across scan planes that are significantly larger in physical extent than the measurement system.

Crucially, the plane-polar (and plane bi-polar) geometries provide additional scope for suppressing range multipath that are not typically available when using conventional plane rectilinear implementations. As the integrity of the measurement can be compromised in a large part by range reflections, *i.e.* clutter, which are often found to constitute one of the largest contributors to the overall facility level error budget [4] this can constitute a very attractive attribute. This paper will examine the use of a number of existing multipath suppression techniques which are used to enhance the signal to stray signal ratio, such as conventional and alternate plane redundant measurements, aperture plane spatial filtering, and will for the first time demonstrate the extension of sophisticated mode orthogonalisation and filtering techniques to the plane-polar geometry [5, 6]. This paper presents an overview of the processing before proceeding to present and discuss range measurements that verify its effectiveness.

2. Introduction to Plane Polar Near-Field Antenna Measurements

It is widely known that an angular spectrum of plane waves can be obtained directly from the sampled tangential near-field components using [1, 7],

$$\underline{F}_T(k_x,k_y)=\int_{-\infty}^{\infty}\int_{-\infty}^{\infty}\underline{E}_T(x,y)e^{j(k_x x+k_y y)}dxdy \qquad (1)$$

It is also known that, from an application of the stationary phase algorithm [7], the asymptotic far electric fields can be easily obtained from the angular spectrum since as $r\to\infty$ [1, 7],

$$\underline{E}(k_x,k_y)\approx j\frac{e^{-jk_0 r}}{\lambda r}\frac{k_z}{k_0}\left[\underline{F}_T(k_x,k_y)-\frac{\underline{k}_T\cdot\underline{F}_T(k_x,k_y)}{k_z}\hat{\underline{e}}_z\right] \qquad (2)$$

Through the use of a multidimensional exchange of variables, it turns out to be a comparatively straightforward task to recast Equation (1) in a form that is directly applicable to the plane-polar measurement system where the samples are taken on a plaid, monotonic

and equally spaced plane-polar grid. In this case the transformation from Cartesian to plane bi-polar co-ordinates is a one-to-one mapping, the analytic functions are continuous, the necessary partial derivatives exist and are continuous, and assuming the initial condition is specified in a plane-polar co-ordinate system where the condition that $r \geq 0$ applies (this is not a practical limitation) such that $x = r\cos\phi$, $y = r\sin(\phi)$, with $z =$ arbitrary but fixed, the Jacobian can be expressed as [7],

$$\frac{\partial(x,y)}{\partial(r,\phi)} = \begin{vmatrix} \frac{\partial x}{\partial r} & \frac{\partial x}{\partial \phi} \\ \frac{\partial y}{\partial r} & \frac{\partial y}{\partial \phi} \end{vmatrix} = \begin{vmatrix} \cos\phi & -r\sin\phi \\ \sin\phi & r\cos\phi \end{vmatrix} = r \tag{3}$$

Hence,

$$F(k_x,k_y) = \int_0^{2\pi}\int_0^{\infty} f(r,\phi) e^{jk_0 r(u\cos(\phi)+v\sin(\phi))} r dr d\phi \tag{4}$$

Finally, the transformation from plane-polar to Cartesian unit vectors, and therefore also field components, can be expressed as,

$$\underline{\hat{e}}_x = \cos\phi\,\underline{\hat{e}}_r - \sin\phi\,\underline{\hat{e}}_\phi \tag{5}$$

$$\underline{\hat{e}}_y = \sin\phi\,\underline{\hat{e}}_r + \cos\phi\,\underline{\hat{e}}_\phi \tag{6}$$

Thus, the Cartesian components of the angular spectrum of plane waves can be obtained directly from the plane-polar electric field components sampled on a regular plane-polar grid. The corresponding near-fields can be recovered from the plane wave spectrum (PWS) from an inversion of equation (1) [7],

$$\underline{E}(x,y,z) = \frac{1}{4\pi^2}\int_{-k_{y0}}^{k_{y0}}\int_{-k_{x0}}^{k_{x0}} \underline{F}(k_x,k_y,z=0) e^{-jk_0(ux+vy+wz)} dk_x dk_y \tag{7}$$

Here, $k_{x0} = k_{0y} = 2\pi/\lambda$. When implemented numerically, the infinitesimal area of a sector of the plane-polar grid in (4) must be replaced with a finitely small elemental area. When the angle θ is in units of Radians, the area A of a sector can be expressed as,

$$A = r^2\theta/2 \tag{8}$$

Thus, the elemental segment area of each sample is,

$$A = \frac{\theta}{2n}\left[(r+\delta/2)^2 - (r-\delta/2)^2\right] = r\delta\theta/n \tag{9}$$

Here, r is the radius of the sample, δ is the sample spacing, θ is the sector angle in radians, and n is the number of samples in each "ring". The centre point is a special case with an elemental area of,

$$A = \frac{\text{Area of sector}}{n} = \frac{1}{2n}\left(\frac{\delta}{2}\right)^2\theta = \frac{\delta^2\theta}{8n} \tag{10}$$

The near-field probe can be conceived of as being a device that spatially filters the fields received from different parts of the AUT. It is not usually possible to neglect these effects in a planar range because of the large angles of validity required, and the comparatively short measurement distance employed. The necessary expressions required to correct the measured near-field data for the directive properties of the measuring probe, can be shown to be [7],

$$[A] = \frac{\lambda}{j}[M]^{-1}\cdot[P]^{-1}\cdot[S]e^{jk_z z_0} \tag{11}$$

Here, the matrix [A] is used to denote the probe corrected fields of the AUT, the matrix [S] are the angular spectra derived from the measured near-field. Here, k_z is the z directed components of the propagation vector, and Z_0 is the AUT-to-probe separation.

Incorporating the probe pattern correction within the near-field to far-field transform developed above commences by recognising that the AUT-to-probe coupling will change differentially from linear scan to linear scan as the AUT is rotated in ϕ across the acquisition interval. Hence, as the probe polarisation rotation angle depends directly on ϕ, the task of applying probe pattern correction has to be moved inside of the double integral of Equation (4) with the linear integration being evaluated first. In order that the probe pattern correction technique can be extended to accommodate the case where the probe has been rotated by an arbitrary, but fixed, angle ϕ about the positive z-axis of the range all that is required is to rotate the pattern of the probe and the pattern of the, output, infinitesimal Hertizan dipole, and then to resolve the corrected fields back onto the range polarisation basis. A detailed verification of this can be found in [7, 8]. In this way, probe corrected far-field data can be obtained with no loss in rigour. Although this approach still requires the use of approximation, *i.e.* interpolation, in the preparation of the rotated probe pattern, the probe pattern is typically grossly over sampled, and by design will be a low gain, slowly varying far-field pattern function which is easily approximated by piecewise polynomial fitting. Or, alternatively, it could be obtained from analytic models in the event simple open ended rectangular waveguide probes are employed [9].

3. Introduction to Planar-MARS

A complete and detailed description of the Planar MARS (P-MARS) transformation and post-processing algorithm is beyond the scope of this paper. However, an overview of the novel processing algorithm is presented below with a more detailed mathematical treatment being left to the open literature [5, 6]:

1. Calculate the probe corrected far electric field form near-field measurements with the AUT offset from the origin of the measurement co-ordinate system.
2. Apply a differential phase change to mathematically translate the AUT to the measurement system origin.
3. Obtain the translated mode coefficients of the AUT for an AUT conceptually located at the origin of the measurement co-ordinate system.
4. Apply band-pass filtering function to suppress unwanted higher order mode coefficients where the

properties of the filter function are determined from the physical size of the AUT.

5. Compute the complete P-MARS filtered far electric field pattern from the filtered mode coefficients.
6. Repeat steps 3 to 5 inclusive applying the mode filtering to the orthogonal axis.

In principle, it is possible to obtain spherical mode coefficients (SMC) [6] or cylindrical mode coefficients (CMC) [5] from the PWS by field matching outside the excluded region. However, due to their greater numerical stability and the enormous ease and efficiency with which they can be obtained from far electric fields, in this case it was preferable to work with CMCs.

4. Overview of Plane-Polar Validation Results

This section presents a summary of the verification of the plane-polar transformation. In order that the plane-polar near-field to far-field transform with general probe pattern correction could be verified, a slotted waveguide *x*-band planar array antenna was acquired using an NSI-300V-12x12 vertical plane rectilinear near-field scanner and separately using an NSI-920PP-6 horizontal plane-polar near-field scanner. In each case a WR90 open ended rectangular waveguide (OEWG) probe was used with the AUT-to-probe separation kept consistent. These systems can be seen presented in Figures 1 and 2. The 920PP-6 uses a 3' (0.9 m) linear travel stage above an azimuth rotator to provide the scanning motion. However, with the use of this linear stage combined with the azimuth rotator, a maximum effective scanning area of 6' (1.8 m) diameter can be achieved. As can be seen from inspection of Figure 3 and 4 the respective far-field co-polar patterns are in very encouraging agreement. Here, the patterns have been presented in the form of false colour checkerboard plots with the pattern tabulated on a plaid monotonic and equally spaced direction cosine grid, with the electric fields resolved onto a Ludwig II azimuth over elevation polarisation basis [7]. When examining these results, it is important to recognise that the plane-rectilinear and plane-polar measurements were taken using completely different test systems which were installed within separate chambers. Thus, the differences in low level, wide out, patterns are most likely a result of differences in scattering between the respective measurements. The plane-rectilinear system was housed in a partially absorber lined chamber; whereas the plane-polar system had some metallic surfaces exposed thereby increasing the scattering in some localised directions. Although not shown, the agreement attained between the respective cross-polar patterns was similarly encouraging with only small differences being observed on boresight which resulted primarily from the use of a theoretical probe pattern for the correction [9] which was not able to take account of imperfections in manufacture *etc.*, which impacted on the polarisation purity of the realised probe.

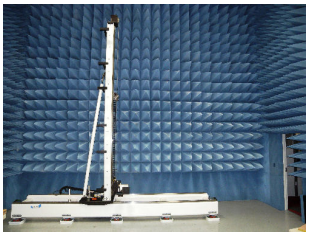

Figure - 1 NSI-300V-12x12 vertical plane rectilinear system.

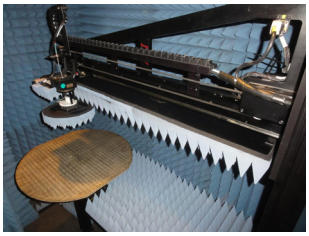

Figure 2 - NSI-920PP-6 horizontal plane polar system.

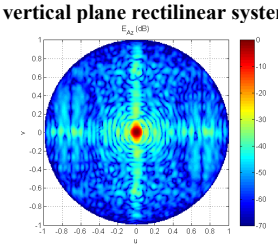

Figure - 3 Far field power pattern from plane rectilinear measurement.

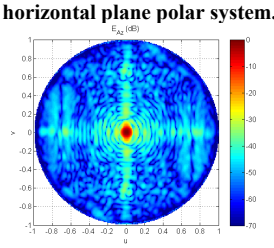

Figure 4 - Far-field power pattern from plane-polar measurement.

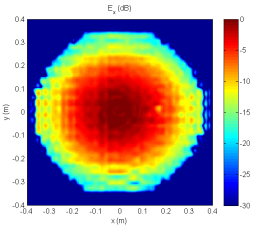

Figure 5 - Aperture illumination amplitude function from plane rectilinear measurement

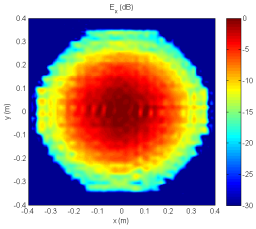

Figure 6 - Aperture illumination amplitude function from plane-polar measurement

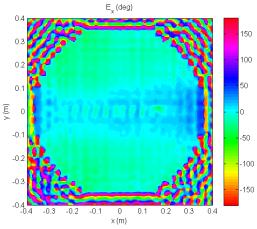

Figure 7 - Aperture illumination phase function from plane rectilinear measurement

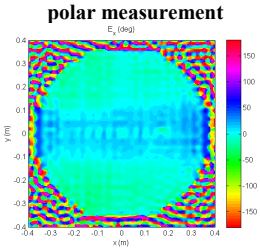

Figure 8 - Aperture illumination phase function from plane-polar measurement

By way of further validation, Figure 5, and 6 contain respectively, the reconstructed aperture illumination function of the waveguide array as obtained from planar and plane-polar near-field testing. Similarly, Figure 7 and 8 contain equivalent phase functions. From inspection of these figures it is clear that the agreement is very encouraging. The underlying functional form of the respective amplitude and phase patterns are the same with the very slight difference in horizontal phase taper that is evident between the plane-rectilinear and plane-polar holograms indicating slight azimuth misalignment of the AUT when it was installed in the plane-rectilinear range. The verification of the critically important rotated probe pattern correction technique has been established previously, *e.g.* see [7, 8], thus this aspect of the technique is left to the open literature. The next section is

devoted to examining the use of plane-polar multipath suppression.

5. Plane-Polar Reflection Suppression

Plane-polar measurements can be taken using several different, acquisition types:

1) $0 \le r \le r_{MAX}$, $-\pi \le \phi \le \pi$, (conventional plane),

2) $-r_{MAX} \le r \le 0$, $-\pi \le \phi \le \pi$, (alternate plane),

3) $-r_{MAX} \le r \le r_{MAX}$, $-\pi \le \phi \le \pi$, (redundant).

Case 3 above requires the ϕ-axis to intersect with the centre of the linear translation stage as illustrated in Figures 12 and 13. Conversely, Figure 2 shows the ϕ-axis in the usual position used for plane-polar measurements (*i.e.* Case 1) where negative r motion is not possible. Here, when the angles are in radians, the mapping from the "alternate" (or second) plane to the conventional (or first) plane can be expressed mathematically as, $r \rightarrow -r$ and $\phi \rightarrow \phi \pm \pi$. Clearly, by allowing ϕ to vary by more than modulo 2π or alternatively, to allow the polar angle to be centred about a value other than zero, an infinite number of other, trivial, representations become available but these offer no additional utility and are not considered herein. Although each of these schemes acquires the same scan area, the position of the AUT and the probe within the range when the data was acquired is *different*. This therefore provides a simple way to assess, and potentially, supress chamber multipath, *i.e.* clutter. Figure 9 contains a comparison of the conventional and alternate planes (with the alternate plane x-polarised electric near-field data having been mapped into the conventional plane) for the case of an x-band slotted waveguide planar array antenna of approximate diameter 10" (0.254 m). Here, the patterns have been plotted tabulated on a plaid monotonic plane-polar grid with the near-field being acquired with the probe counter rotated (in a Ludwig III type acquisition scheme [7]) so that the AUT and probe field remain polarisation matched throughout the near-field scan. Differences between the respective red (conventional) and black (alternate) contours primarily result from range reflections. A quantitate measure of the similarity between the measured data sets can be found presented in Figure 10 which contains a plot of the equivalent multi-path level (EMPL) [7]. The EMPL is half the absolute difference between the patterns expressed in dB and can be thought of as the amplitude necessary to force the two different pattern values to be equal. Here, the differences which result primarily from range clutter peak at the circa -30 dB level with respect to the peak of the pattern. As there are no systematic differences evident it is possible to confirm that measurement errors resulting from imperfections in range alignment (r = 0 offset error), backlash, or drift are minimal and can be ignored for the purposes of this comparison exercise. As this measurement is over determined, (*i.e.* containing "redundant" data) it constitutes an excellent candidate for verifying the effectiveness of clutter suppression techniques.

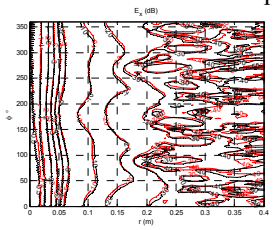

Figure 9 – Comparison of conventional (red) and alternate (black) near-field data.

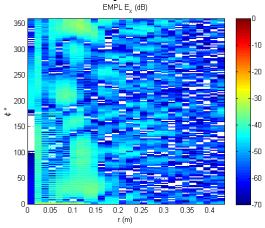

Figure 10 – EMPL comparison of conventional and alternate near-field data.

Clearly, it is possible to obtain far-field data using: the conventional plane, the alternate plane, and the average of the two data sets where the averaging process can be used to supress the effects of range reflections. However, although a viable strategy, this would result in a doubling of the measurement time which undesirable in many areas of application. Alternatively, as the AUT is an "aperture antenna", it is possible to perform a back propagation of the radiated near-fields to the antenna aperture plane (*i.e.* that infinitesimal planar interface between the conduction current and the displacement current being the majority carrier) using equation (7), before applying a two-dimensional band pass spatial filter function so as to set the fields outside of the antenna's aperture plane to zero whereupon the filtered far-field pattern can be recovered [10, 5]. Lastly, the P-MARS mode orthogonalisation and filtering algorithm can be harnessed to obtain multipath supressed far-fields [5, 6]. Here, the same AUT dimensions (height and width) were used for both P-MARS and aperture plane filtering. Using these techniques it is possible to compute a number of different far-field data sets from the single near-field acquisition. These can be seen plotted in Figure 11 in the form of an azimuth pattern cut.

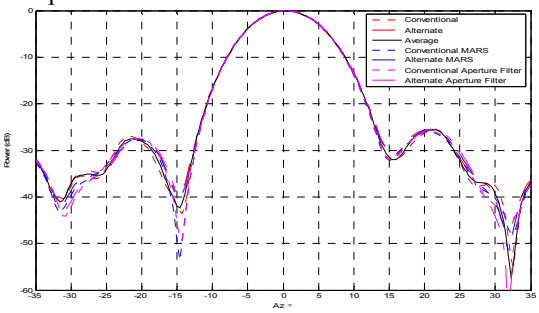

Figure 11 – Comparison of far-field azimuth cuts obtained using various multi-path suppression techniques.

Here, the range of the angular axis has been determined from the angular onset of the first order truncation effect which limits the azimuth and elevation field of validity to approximate 35° as measured away

from boresight with this being determined from the radius of the AUT, the length of the linear scanning axis, and the AUT-to-probe separation distance [7]. Here, the red traces denote the far-field pattern obtained from standard plane-polar processing, the blue traces denote P-MARS processed far-field patterns, magenta traces denote aperture filtered far-field patterns, and the black trace is obtained from the vector average (*i.e.* with due regard to phase) of the conventional and alternate measurements.

From inspection, of this plot and others (not shown), it is clear that all seven pattern cuts are in broad general agreement and although some differences are evident it is a challenging task to derive very many specific conclusions. Thus, as the patterns are similar and since there is a great deal of data to be examined, *i.e. circa* 40,000 data points within each individual far-field pattern within the angular region defined by truncation, it was decided that the use of an objective quantitate measure of similarity would aid the analysis. In this case, the ordinal measure of adjacency was employed. A detailed description of this comparison technique can be found in the open literature [7]. Here, the correlation coefficient is symmetrical and normalised so that $k = 1$ represents a perfect correlation, whereas $k = 0$ represents no correlation. A number of useful comparisons can be formed and these are summarised in Table 1 where each test comprises assessing approximately 80,000 individual data points that fall within the far-field angle of validity.

Test	I_1	I_2	**Ordinal** $k(I_1,I_2)$
1.	Conventional	Alternate	0.8122
2.	Conventional	Average	0.9016
3.	Alternate	Average	0.9069
4.	Conventional with P-MARS	Alternate with P-MARS	0.8312
5.	Conventional with Aperture filtering	Alternate with Aperture filtering	0.8415
6.	Conventional with P-MARS	Average	0.8931
7.	Conventional with Aperture filtering	Average	0.8789

Table 1 – Comparison of similarity between far-field patterns.

Test 1 consisted of comparing the two-dimensional far-field pattern as obtained from the conventional and alternate planes. The k value of 0.8122 represents a measure of the similarity between the measurements where the difference between this value and unity is primarily a measure of the impact resulting from range multipath. By way of a check, as the geometric average should lie between these two measurements, the agreement between the average and each measurement should be better and indeed this is confirmed by the larger k value obtained in Tests 2 and 3. As both P-MARS and the aperture spatial filtering algorithms aim to remove artefacts arising from scattering, and these are assumed to be the principal causes for the differences observed between the conventional and alternate results, the agreement between the respective filtered patterns should be better than that which was obtained in Test 1. Here, as $k = 0.8312$ the P-MARS processed conventional and alternate patterns (Test 4) are found to be in better agreement than had been the case without P-MARS processing (Test 1) for which $k = 0.8122$. However, the agreement between the aperture filtered conventional and alternate planes was slightly better as in Test 5, $k = 0.8415$. This would perhaps indicate that the aperture filtering technique was more effective at filtering out range multipath than the corresponding P-MARS technique. However, the situation is more complicated than this. If one compares the P-MARS processed patterns to the average (which can be taken to represent a "truth" model) as in Test 6 where $k = 0.8931$, one finds that the P-MARS processed patterns are in better agreement, than when one compares the aperture filtered results with the averaged results as in Test 7 where $k = 0.8789$. This indicates that although the conventional and alternate aperture filtered results are in close agreement with one another, they are in less good agreement with the averaged far-field pattern. Thus the aperture filtering has materially affected the form of the processed patterns. By examining the far-field patterns this could be seen to be a consequence of a spurious ripple that was introduced by the tight aperture plane filtering function. It is well known that the exact form of a resulting transformed spectrum can be largely dependent upon (and sensitive to) changes in the fields at the extremities of a band pass spatial filtering function. To a large part, this is what we are encountering here. Although it is possible to utilise a broader filter function, this would then not represent a like for like comparison with P-MARS and opens up the question of how in practice one would best select the optimal value for the spatial filter function.

As a further test, it was decided that the effectiveness of the P-MARS processing would be examined by making repeat measurements where the chamber reflections would be changed with the introduction of a known scatterer. To illustrate this, Figure 12 contains a picture of the plane-polar system when acquiring baseline measurements of the waveguide array. Conversely, Figure 13 contains a picture of the same system with a reflecting plate having been installed within the chamber so as to significantly increase the amount of chamber multiple reflections. The P-MARS processed far-field patterns were obtained using the post-processing algorithm presented above and the resulting x- and y-axis cylindrical mode coefficients (CMC) can be seen plotted in Figures 14 and 16 respectively for the baseline case. CMCs are complex numbers that are functions of the polarization index s, the ϕ index n and the Fourier variable γ with these figures comprising false colour, checkerboard, plots of the normalised amplitudes of the

CMCs modes for $s = 1$, *i.e.* B^1 [5]. Figures 15 and 17 contain analogous CMC plots for the case when the reflecting plate had been installed within the chamber. From inspection of Figures 15 and 17, it is clear that the amount of power contained within higher order modes that are not attributable to the AUT, *i.e.* those modes outside of the black ellipse described by $n^2 + (\gamma a)^2$ [5], is significantly higher for the case where the reflecting plate had been installed in the chamber, as depicted within the directly comparable Figures 14 and 15. Some higher order modes are evident within the baseline case, particularly Figure 16. This was anticipated and arises from inherent range reflections as indicated from the differences observed between conventional and alternate plane measurements examined above. It is perhaps worth noting that in the examples presented within this paper, a sharp Dirichlet window was adopted. More sophisticated windowing functions are available however, and their use has been examined in this area of application, *c.f.* [11].

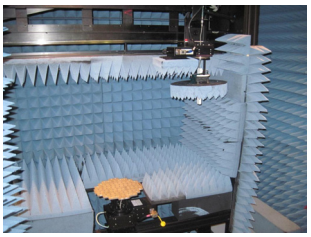

Figure 12 – Plane polar system acquiring baseline measurement.

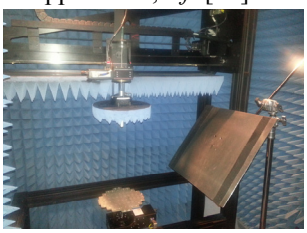

Figure 13 – Plane polar system with reflecting plate installed.

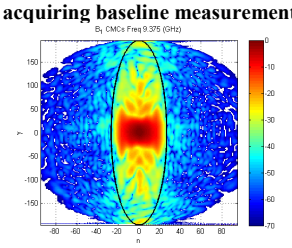

Figure 14 – *x*-axis CMCs without reflecting plate

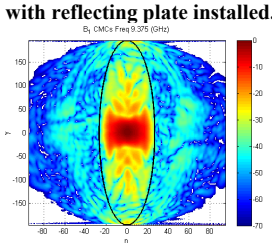

Figure 15 – *x*-axis CMCs with reflecting plate

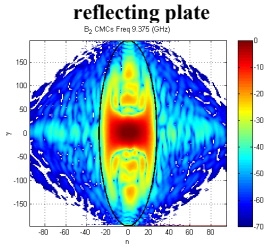

Figure 16 – *y*-axis CMCs without reflecting plate

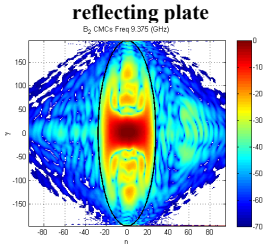

Figure 17 – *y*-axis CMCs with reflecting plate

The far-field great circle azimuth and elevation cardinal cuts which can be seen pretend in Figures 20 and 22 respectively for the baseline (red traces) and scattering contaminated (black traces). These far-field patterns were obtained from standard plane-polar processing, *c.f.* [2, 7]. A quantitative measure of the similarity, or adjacency, between the patterns can be obtained by evaluating the EMPL which is depicted by the magenta trace. Figures 21 and 22 contain equivalent P-MARS processed azimuth and elevation pattern cuts. Here, it is evident that the respective baseline and reflector contaminated traces are in better agreement. This is also confirmed by the reduction in the EMPL which can be seen to have reduced by *circa* 5 to 10 dB.

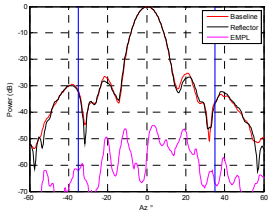

Figure 18 – Far-field Az cut with and without reflector.

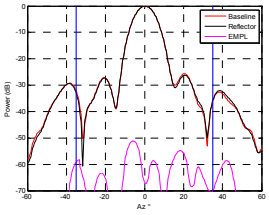

Figure 19 - Far-field Az cut with & without reflector with MARS.

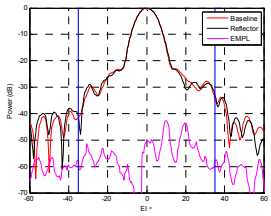

Figure 20 – Far-field El cut with and without reflector.

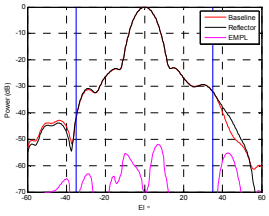

Figure 21 - Far-field El cut with & without reflector with MARS.

Unlike the plane rectilinear acquisition system, the plane-polar system as implemented here rotates the AUT during the course of an acquisition. In principle, this enables the AUT to be offset from the centre of that rotation much in the same way as is customary when taking spherical or cylindrical MARS measurements. So that the impact that this would have on the effectiveness of the P-MARS post processing a custom bracket was used so as to enable an offset AUT measurement to be taken. As usual with a MARS type measurement, a 10.25" (0.26 m) tangential offset was used which was comparable with the 10.8" (0.274 m) diameter of the aperture of the AUT. It would have been preferable for the offset to have been slightly larger than this, but that would have resulted in an overly truncated near-field measurement. This configuration can be seen presented in Figure 22, with the resulting *x*-polarised plane-polar near-field data which has been plotted in rectangular Cartesian form in Figure 23.

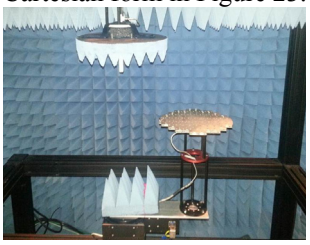

Figure 22 – Plane-polar system with AUT offset tangentially.

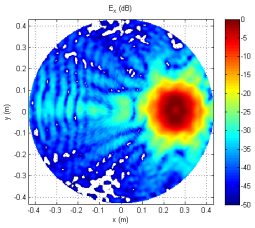

Figure 23 – Acquired near-field data of AUT with reflector.

Here, it is clear that the offset has resulted in the near-field data being truncated in the $-30° \leq \phi \leq 30°$ range as the field has decreased to perhaps as little as *circa* -30 dB from the peak of the near-field pattern at the perimeter of

the sampling interval. Such truncation will reduce the angle at which the first order truncation effect onsets, particularly in the azimuth axis, and will introduce some pattern ripple as a result of spectral leakage at all angles. As before, two measurements were taken. Firstly, the AUT was acquired offset by 10.25" (0.26 m) radially from the ϕ-axis with no scatterer present, and secondly with the AUT in the same position but with a scatterer introduced on the positive r side of the plane-polar scanner, *i.e.* in a similar location to that shown in Figure 13. The far-field great circle azimuth pattern cut for the cases of measurements with, and without, the scatterer can be seen plotted in Figure 24 together with the EMPL. The equivalent P-MARS processed patterns can be seen presented in Figure 25. Here, although the amount of scattering coming from the reflecting plate has decreased from that which was observed during the previous trial, *c.f.* -55 dB EMPL level in Figure 24 with the -46 dB level seen in Figure 18, the P-MARS processing has still significantly improved immunity of the measurement to range reflections by a further 10 dB or more in the main beam region despite the small AUT-to-probe separation of 7" (0.18 m, 5.5λ). Additionally, the spurious high angular frequency ripple that was initially very evident on the far-field patterns has been effectively suppressed. The ability to apply P-MARS processing in this fashion with such a reduced range length, and therefore with minimal truncation, is peculiar to the plane-polar (& plane-bipolar) measurement techniques as ordinarily P-MARS processing requires an offset of an AUT diameter in the Z-axis.

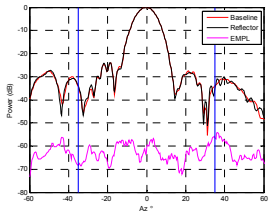

Figure 24 - Far-field Az cut with & without reflector.

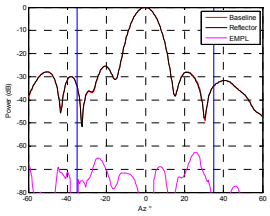

Figure 25 - Far-field Az cut with & without reflector with MARS.

6. Summary and Conclusions

This paper reports the first successful application of the MARS measurement and post-processing technique with a plane-polar near-field antenna test system. MARS processing can be used with a very high degree of confidence since all the steps in the measurement and analysis are consistent with the well-established principles of standard near-field theory and measurement technique, and all comparisons to date have proved *overwhelmingly* positive. The translation of the far-field pattern to the origin with the application of a differential phase shift is rigorous. The selection of the mode cut-off for the translated pattern is based on the physical dimensions of the AUT and its translated location. The results of the P-MARS processing will reduce, but cannot entirely eliminate, the effect of the scattering. The final result with MARS processing can be degraded if the sampling of the near-field data is too coarse, but this is also true for regular planar processing with, importantly, this parameter being controlled by the user. The P-MARS measurement and post processing scheme holds for general source geometries, unlike the aperture plane spatial filtering technique that requires a "thin" antenna, and has been found to be robust with respect to truncation of the measured near-field data, both within this paper and previously [6], and can be used to achieve acceptable results with the use of minimal absorber. Uniquely, P-MARS can be successfully deployed at reduced range lengths providing the AUT can be offset tangentially from the origin of the plane-polar (or bi-polar) system.

As this paper has recounted the preliminary results of an on-going programme of research, the planned future work is to include implementing an alternative spherical mode expansion based post-processing algorithm, *c.f.* [6], to obtain further separate confirmation of these results.

7. REFERENCES

[1] D.M. Kerns, "Plane-Wave Scattering-Matrix Theory Of Antennas And Antenna-Antenna Interactions", Nat. Bur. Stand. (U.S.) Monograph 162, June 1981.

[2] V. Galindo-Israel, Y. Rahmat-Samii, R. Mittra, "A Plane-Polar Approach For Far-Field Reconstruction From Near-Field Measurements", Int. IEEE / AP-S Symp., Seattle, June, (1979).

[3] Y. Rahmat-Samii, L.I. Williams, R.G. Yaccarino, "The UCLA Bi-Polar-Near-Field Antenna-Measurement and Diagnostics Range", IEEE Antennas and Propagation Magazine, Vol. 37, No. 6, December, pp. 16-35, (1995).

[4] A.C. Newell, "Error Analysis Techniques for Planar Near-field Measurements", IEEE Transactions on Antennas and Propagation, vol. AP-36, pp. 754-768, June 1988.

[5] S.F. Gregson, A.C. Newell, G.E. Hindman, M.J. Carey, "Extension of The Mathematical Absorber Reflection Suppression Technique To The Planar Near-Field Geometry", AMTA, Atlanta, October 2010.

[6] S.F. Gregson, A.C. Newell, G.E. Hindman, "Advances In Planar Mathematical Absorber Reflection Suppression", AMTA, Denver, Colorado, October 2011.

[7] S.F. Gregson, J. McCormick, C.G. Parini, "Principles of Planar Near-Field Antenna Measurements", The Institution of Engineering and Technology, UK, 2007.

[8] S.F. Gregson A.J. Robinson, "An Inter-range Comparison in Support of the Characterisation of Space Antenna Systems and Payload Testing", IEE Colloquium on Antenna Measurements 19th June 1998.

[9] A.D. Yaghjian, "Approximate Formulas for the Far Field and Gain of Open-Ended Rectangular Waveguid", IEEE Transactions On Antennas And Propagation, Volume AP-32, No. 4, April 1984.

[10] O.M. Bucci, G. D'Elia, M.D. Migliore, "A General and Effective Clutter Filtering Strategy in Near-Field Antenna Measurements", IEEE Proc.-Microwave Antennas and Propagation, Vol. 151, No. 3, June 2004.

[11] S.F. Gregson, J. McCormick, B.J. Kerse, A.C. Newell, G.E. Hindman, "Computational and Experimental Verification of Far-Field Mathematical Absorber Reflection Suppression", the 6th EuCAP, Prague, March 2012.